Appendix B

Analysis of the flares of Mkn 421 in 2001

In chapter 1 and A the necessary foundation was established to now discuss the analysis of the Mkn 421 data. This data was recorded between ***February 2001 and May 2001*** when Mkn 421 exhibited large flares. The total observation time amounts to 249 hours.

Two main characteristics will be examined. One is the lightcurve which contains ***timing information*** of the flares and time correlations to x-ray measurements. The second concerns the ***spectral properties*** of the flux. Calculated will be the total average spectrum and the spectrum in different flare states including hardness ratio changes.

B.1 Light curve and timing of the flares of Mkn 421

In this section, the measurement of the lightcurve using the ***CT1 telescope*** and other instruments like the ***x-ray satellites RXTE*** and ***ASCA*** and the ***CT-system*** telescopes are described and compared. In addition, fundamental timing properties and time correlations are discussed here.

B.1.1 The light curve of Mkn 421 as measured by CT1

The algorithm of the lightcurve calculation was explained in detail in chapter A. The data is ***binned in runs*** which are ***typically of 20 minutes duration***. Smaller binning was disregarded because the statistics would be unacceptably low. The lightcurve of the whole period is shown in Fig. B.2 and the complete night by night set can be seen in Appendix B. Some runs have high fluxes of up to $(10-15)\ 10^{-11}(TeV\,m^2\,s)^{-1}$. The lightcurve exhibits five main observation periods which are interrupted by moon periods during which observations was only restricted possible. In three of these five periods Mkn 421 showed high fluxes. Moon observation data is not included in this plot and was not analyzed in this document. A lightcurve with daily averages was already shown in Fig. A.41.

Estimation of rise and fall times

Measurements taking during twelve days and containing significant flares were selected and are shown in Figures B.3, B.4 and B.5. There is some evidence that some of the flares are faster than the resolution of the run bins. It is difficult to estimate the rise time in some cases. To obtain numbers for the doubling rise time, the halving fall time and the average FWHM duration of a typical flare, ***three*** different approaches were used.

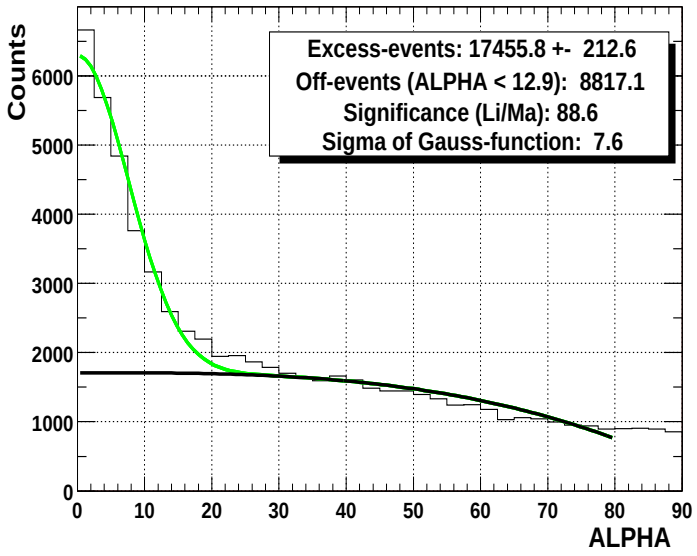

Figure B.1: This figure shows the total excess of the Mkn 421 dataset which amounts to 17400 +- 210 signal events over approximately 8800 background events and which was recorded between February 2001 and May 2001 with a total observation time of 249 hours.

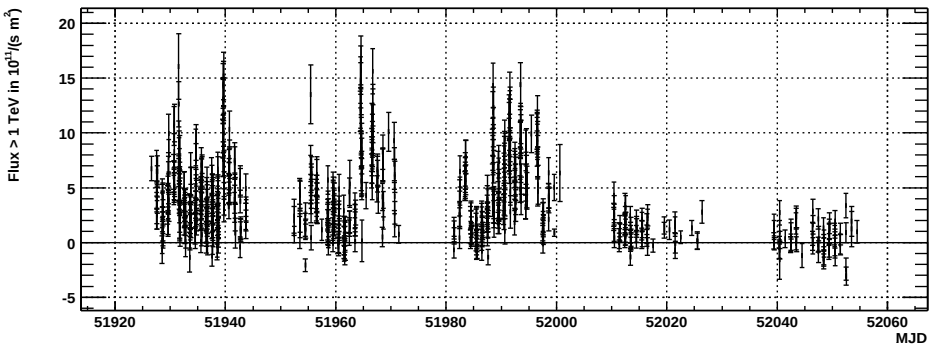

Figure B.2: The light curve for the complete period between February 2001 and May 2001 is shown. Each point corresponds to a single run which is typically of approximately 20 minutes duration.

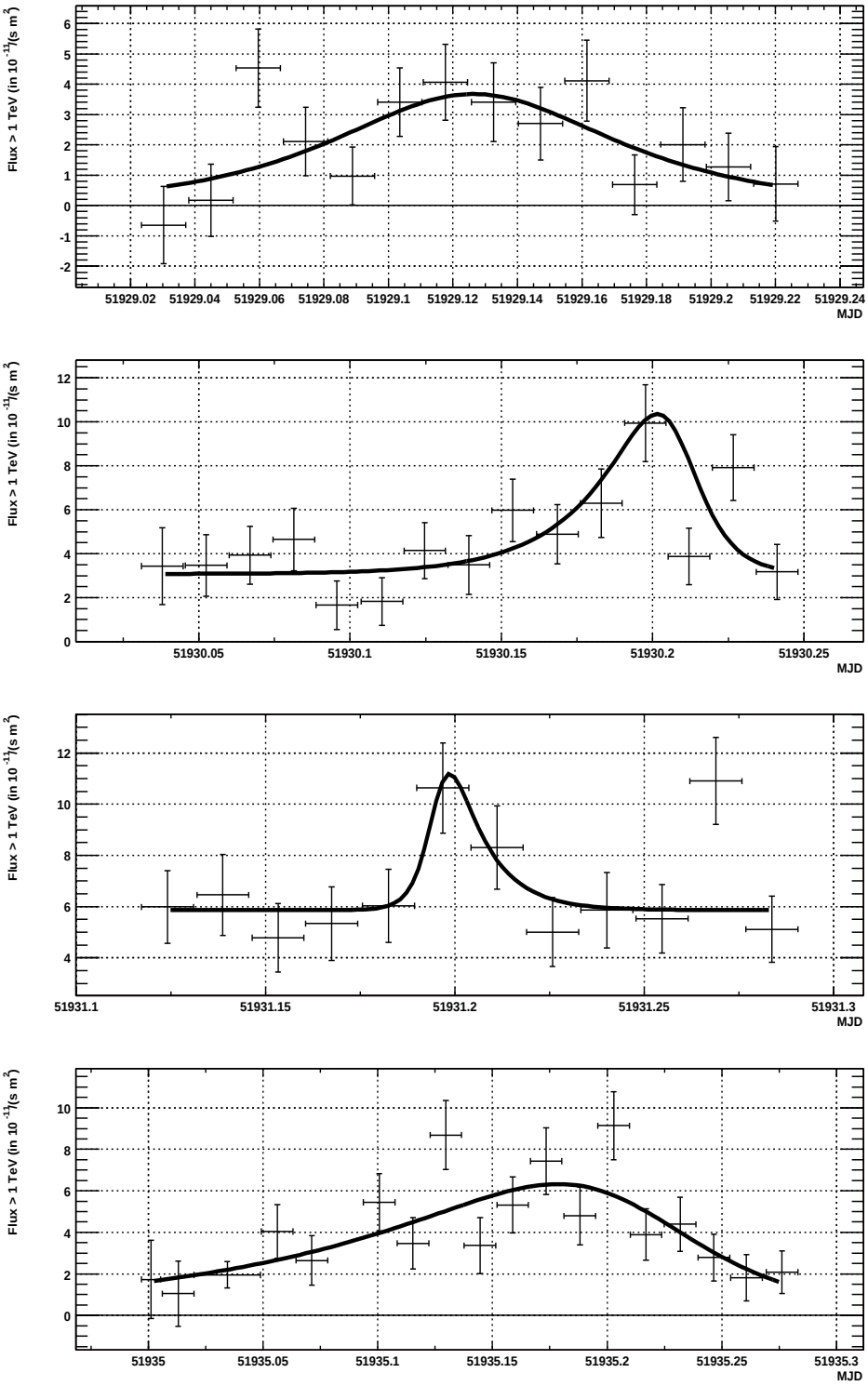

Figure B.3: Selected flux measurements from the nights 51928, 51929, 51930 and 51934. The flares have been fitted with a simple flare model described below.

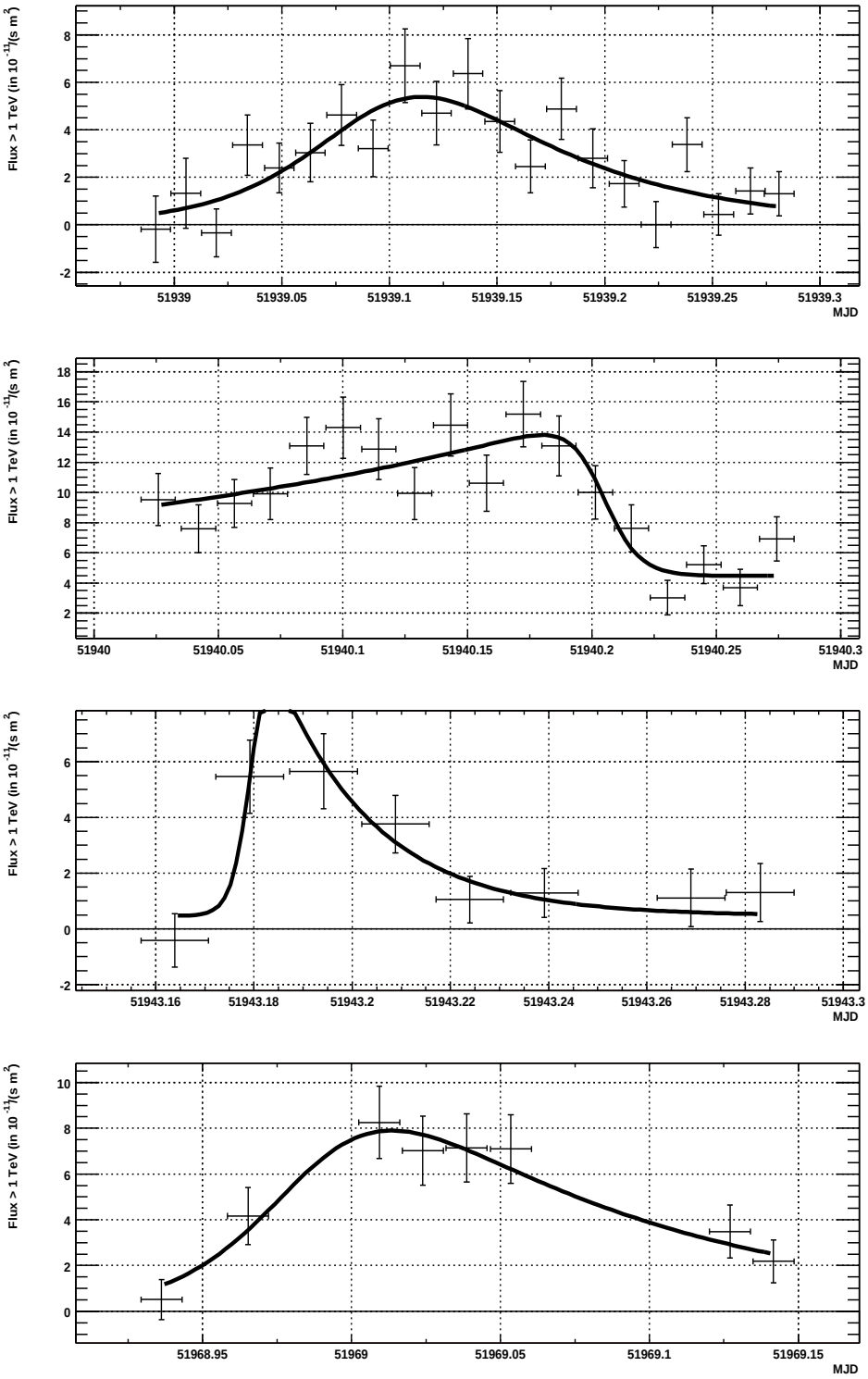

Figure B.4: Selected flux measurements from the nights 51938, 51939, 51942 and 51968. The flares have been fitted with a simple flare model described below.

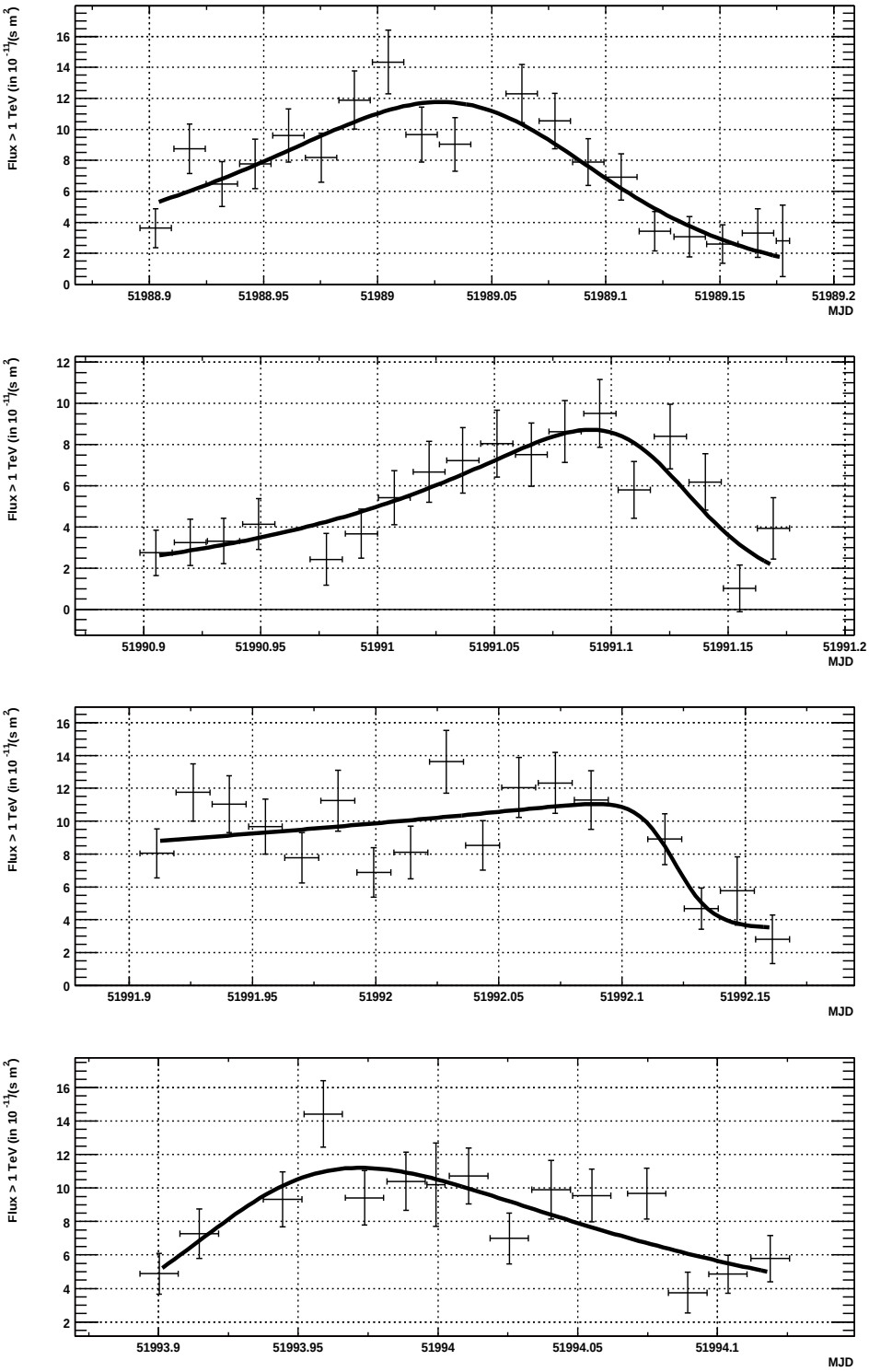

Figure B.5: Selected flux measurements of the nights 51988, 51990, 51991 and 51993. The flares have been fitted with a simple flare model described below.

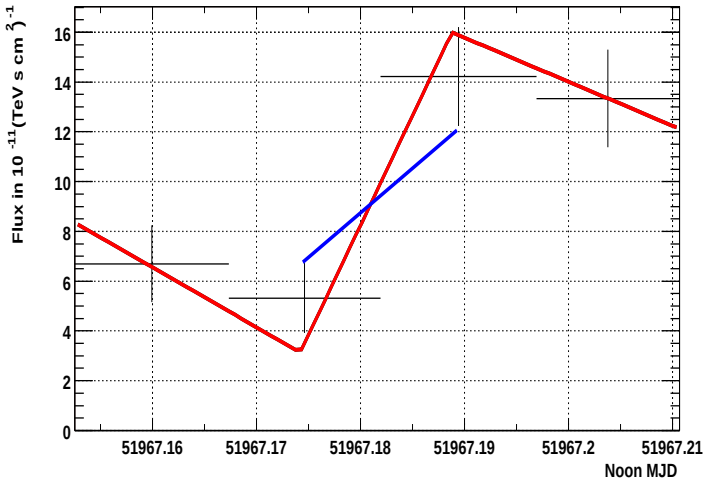

Figure B.6: Fit to obtain the doubling time. The flare taken occurred in the night 51967. It shows a doubling time of 8.2±7.0 minutes. Even the worst case scenario (blue line) still has a doubling time of only 23 minutes.

1. For a simple characterization, ***a flare model*** has been fitted to each night.

$$F(t) = a + \frac{b}{2^{\frac{(t-t_0)}{c}} + 2^{-\frac{(t-t_0)}{d}}} \tag{B.1}$$

   This function behaves like an exponential in the limits of minus and plus infinity. Rises and falls are supposed to have exponential character (corresponding to sudden outburst and exponential cooling). It has doubling rise and halving fall times c and d. This model assumes that several small fast flares ***pile up*** to a single very large flare. This means that the flare doesn't start from zero but rather from a ***constant background*** which is estimated by a. This fit is used to estimate the average duration of fast flares and the rise and fall times starting from a constant background.

2. For very fast flares ***four points*** are taken with the rise or fall in the middle (see Fig. B.6). Three segments of straight lines are fitted to these four points by ***integrating*** over the run period. In this manner we can approximate the slope of the middle segment by using the information from the points on the left and the right and obtain its error from the fit. The fit contains ***two free parameters*** which are the slopes of the first and second segments. The offset from zero on is given by the first and last point which lay on the first and last straight line. The doubling time is calculated here by assuming the a flare starts from ***zero*** and not starting from an offset as by fitting the flare model. In this way the rise time is calculated ***conservatively***.

3. Since the 4 point fit is not useful in all the cases, the doubling rise time between ***two neighbouring points*** is calculated by means of a ***simple line*** connection between two points. The error is obtained from the errors of the fluxes. Since this method is very sensitive to statistical fluctuations, the doubling and falling times are calculated by taking the ***worst case scenario***. The flux values used are the measured fluxes plus/minus their one sigma errors. (The ends of the error bars are connected, see Fig. B.6).

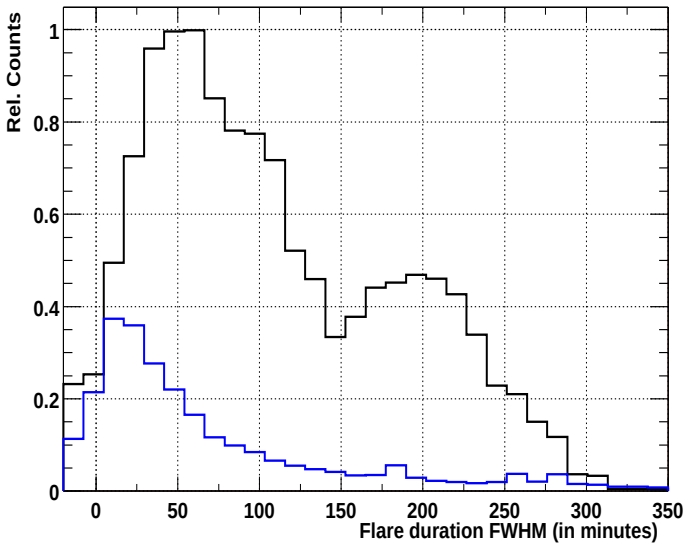

Figure B.7: FWHM duration of 21 large flares obtained by fitting the flare model above. The typical duration for fast flares ranges between ***one hour*** and ***three and a half hours***. The distribution of the duration is obtained by filling ***Gaussian distributions*** into a histogram. The mean and sigma of such an Gaussian distribution corresponds to the measured value and its errors. The ***underlying blue line*** is the ***noise background*** that was obtained by simulating a lightcurve with Gaussian random distributed data points around a mean of the daily average flux. Then the same flare model was fitted as to the real light curve. For each night ***100*** lightcurves were simulated. The blue line shows that for random lightcurves ***significantly less*** flares are found.

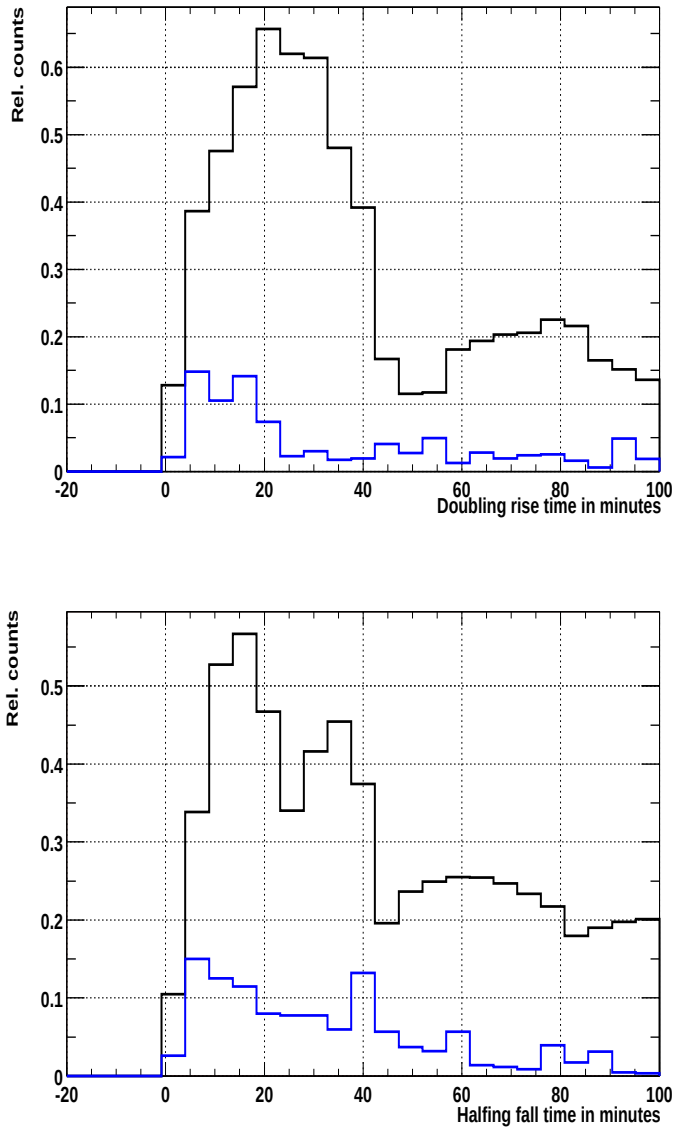

Figure B.8: These two plots show the parameter values c (doubling rise time) and d (halving falling time, see Equ. B.1) obtained from fitting 21 large flares. Typical time scales in this model range from upwards 25 minutes. The distributions are obtained by filling ***Gaussian distributions*** into a histogram. The mean and sigma of the Gaussian distribution corresponds to the measured value and its errors. The ***underlying blue line*** is the ***noise background*** that was obtained by simulating a lightcurve with Gaussian random distributed data points around a mean of the daily average flux. Then the ***same*** flare model was fitted as to the real light curve. For each night 100 lightcurves were simulated. The blue line shows that for random lightcurves ***significantly less*** flares are found.

Type	MJD	Doubling/halfing time (in minutes)
Fall	51967.05	11.7 +- 11.3
Fall	51990.06	14.1 +- 16.3
Fall	51991.12	12.8 +- 14.9
Rise	51934.18	13 +- 10.7
Rise	51956.06	15 +- 15.2
Rise	51967.17	8.24 +- 6.9

Table B.1: The results of the four point, three segment fit are presented here. The shortest fall time is 12.8 +- 14.9 minutes and the shortest rise time is 8.24 +- 6.9 minutes. Taking into account the large errors, there is evidence of flares that have rise and fall times of 15 to 25 minutes.

Fitting the flare model

The starting values for the fit are set as follows: a=average flux during night, a=8.0, c=30 minutes rise time, c=30 minutes fall time and t_0=the position of the highest flux in that night. In order to select nights with significant flares, first a straight line fit is performed. If the reduced chi-square is less then 1.5, $\chi^2/NDF < 1.5$, then the night is not used for the fit of Equ. B.1. The most interesting major flares are shown in Fig. B.3, B.4 and B.5 while the complete set can be seen in Appendix B.

Only fitting values with errors less than 100% are allowed (as a quality selection cut) for the reminder of the process. 21 fitted flares fulfilled this criteria. The plots in Fig. B.8 and Fig. B.7 are obtained by filling area-normalized ***Gaussian distributions*** into a histogram. The mean and sigma of the Gaussian distribution corresponds to the measured value and its error, respectively. In this way, it is possible to graphically illustrate the distribution for only few measurements. In order to estimate the ***significance*** of the obtained result, the same procedure was applied to lightcurves that were generated by a ***Gaussian random generator***. The mean of the Gaussian distribution is the average daily flux and the variance is the error of each data point. For each night 100 lightcurves were simulated and fitted by the same procedure like the real one. The obtained distribution shows that in random distributed lightcurves ***much less*** flares are found and thus the measured rise time distribution is significantly higher than the background.

The ***average duration*** of fast flares ranges from ***one hour*** to ***three and a half hours*** FWHM. The typical doubling rise and halving fall times in this model range from upwards of 25 minutes. A significant difference between rise and fall times is not observed.

Four point-three segment fit

The results of the four point, three segment (three straight lines) fit are presented here. A sample of rise and fall times faster than 15 minutes are listed in Tab. B.1. The flares can be found in the Fig. B.3, B.4 and B.5 by its MJD.

Taking into account the considerable errors on the measurements, there is evidence that there exist flares that have doubling and halving times of only 15 to 25 minutes.

Worst case scenario: Two point straight line connection

Since the four point fit with two free parameters introduces large errors and since not all fast flares have two neighboring points, the rise and fall time were also calculated from a straight line connection, but ***subtracting one sigma*** from each of the two points (the worst case scenario). Some of the points which are faster then 20 minutes are listed in Tab. B.2.

When considering the errors one should take into account that in this ***worst case scenario*** already one sigma had already been subtracted/added on each of the two points and one obtains still a rise time of 8.24 +- 7.0 minutes. Therefore it can be safely stated that

Type	Noon MJD	Doubling/halfing time in minutes
Rise	51932.01	8.31+- 4.9
Rise	51989.90	9.7 +- 6.6
Fall	51929.05	19.4 +- 13.8
Fall	51992.14	9.57 +- 7.5

Table B.2: In this table some fast rise and fall times are listed. They have been calculated out of a two point connection from which one sigma has been subtracted already (worst case scenario, see Fig. B.6). It can be stated that in a few cases the ***doubling rise and halving fall times*** seem to be ***equal or faster than 15 minutes***.

in a few cases the ***doubling rise and halving fall times*** are for sure ***equal or faster than 15 minutes***.

Conclusions from lightcurve, rise and fall time measurements

The lightcurve measurement made by the CT1 telescope shows a ***very fast variability*** of the source. There is evidence that the fastest ***doubling times*** and halving times are ***equal or faster than 15 to 25 minutes.*** The fit of a flare model to the lightcurve shows that the typical ***FWHM duration*** of the fast flares are ***between one hour and three and a half hours*** while in that model the ***typical*** doubling/halving times are approximately upwards of 25 minutes. A significant difference between rise and fall times has not been seen.

In addition, high fluxes of up to $(15 \pm 2) \cdot 10^{-11} TeV^{-1} s^{-1} m^{-2}$ can be observed sporadically during the four months flare period.

B.1.2 Comparison of the lightcurve to the one measured by the CT-system

To test ***redundancy***, the obtained flux was compared with the flux obtained by the ***CT-system***. This could only be done for time-coincident bins. As Mkn 421 is a very rapidly flaring source, if the flux is not measured by both the CT1 and the CT-System exactly at the same time then it cannot be expected that the measured fluxes precisely coincides. This results in a few points that don't fit perfectly in the trend. However, it can be checked whether both measured fluxes are correlated, whether the scale is the same and whether the origins coincide as well. Fig. B.9 shows the correlation of time coincident bins of quarter day size. The measurements are in good agreement. A straight line fit with $y = p0 + p1 * x$ to the data shows that the origins of both telescopes coincide ($p0 \sim 0$). ***The CT1 flux is approximately 13%$\pm$6% lower than that one determined by the CT-System.***

It should be mentioned that a completely different calibration procedure for CT1 and and CT system has been used. In this respect the difference of 13%$\pm$6% is surprisingly good.

B.1.3 The 2 keV-12 keV lightcurve measured by the All Sky Monitor of the RXTE satellite

Flares of February 2001 to April 2001 have also been detected in the ***x-ray domain at 2 keV to 12 keV*** by the All Sky Monitor (***ASM***) of the ***RXTE*** satellite. This allows ***multi-wavelength observations***. Some basic predictions of the SSC model can be tested. It claims that X-rays are produced by synchrotron radiation of said accelerated electrons while the GeV/TeV γ's are produced by inverse Compton upscattering of said x-ray photons.

Unfortunately the measurements of the All Sky monitor are only a few, short, 90 s measurements per day with very poor statistics and big errors. This does not allow precise

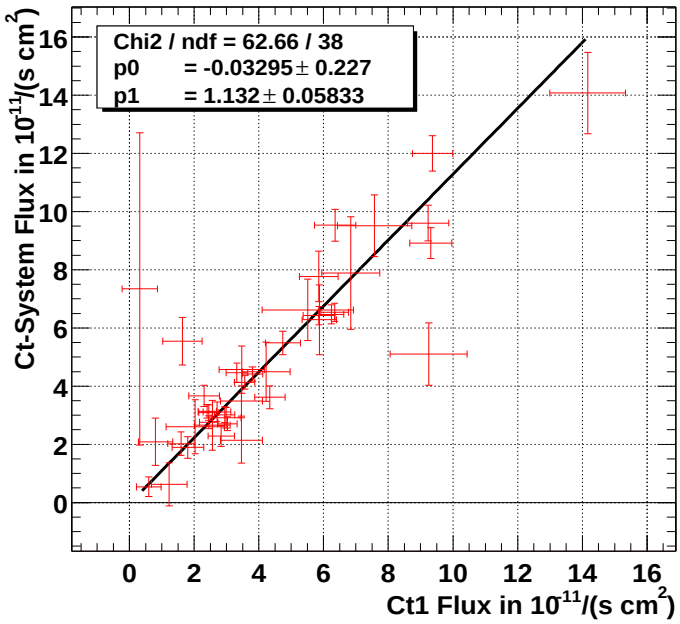

Figure B.9: Correlation of the flux above 1 TeV obtained by the CT-system when compared to the fluxes of CT1 for time-coincident bins of quarter day size. A straight line fit with $y = p0 + p1 * x$ shows that the ***origins of both telescopes coincide*** and that the CT1 flux is approximately ***13% smaller*** than the one of the CT-System. The points which are significantly away from the straight line fit are a result from not completely time coincident measurements of the two instruments.

measurements of the development of the flares. However the measurements can be averaged over bigger time bins. Figure B.10 shows (middle plot) the ASM lightcurve averaged over 12 hour bins and (above) a 24 hour sample of the day 51966. On the small time scale the data is highly noisy. Almost simultaneous points show large differences. If the data is averaged over a bigger time period acceptable results are obtained. In the bottom plot the corresponding CT1 half day bin lightcurve is displayed for comparison. In the next session the time correlation between the two instruments will be discussed in detail.

B.1.4 The discrete correlation function applied to TeV and X-Ray light curves

Looking at Fig. B.10, one may surmise that the fluxes of CT1 and RXTE are correlated with each other. Such a correlation provides very important information about the processes that create x-ray photons and γ-photons.

The empirical correlation function

The ***empirical correlation*** ρ of two vectors F^γ and F^x is generally defined as:

$$\rho = \frac{\sum_i \left(F_i^\gamma - \langle F^\gamma \rangle\right)\left(F_i^x - \langle F^x \rangle\right)}{\sqrt{\sum_i \left(F_i^\gamma - \langle F^\gamma \rangle\right)^2 \sum_i \left(F_i^x - \langle F^x \rangle\right)^2}} \tag{B.2}$$

In our case the situation is more complicated since the measurements are completely non-equidistant distributed in time. Both datasets have been re-binned into ***equidistant*** time bins of size ΔT, as described in Equ. E.35 (Appendix A). The correlation is measured for ***systematic time shifts*** Δt between the two datasets, the flux bins for γ-rays $F^\gamma\left(t_i\right)$ and for x-rays $F^x\left(t_i\right)$, to see if the light of the γ-flares arrives earlier or later than the light of the x-ray flares. Only the time coincident time bins are summed up, using the following formula:

$$\rho\left(\Delta t\right) = \frac{\sum_{t_k = t_i + \Delta t}\left(F^\gamma\left(t_k\right) - \langle F^\gamma \rangle\right)\left(F^x\left(t_i\right) - \langle F^x \rangle\right)}{\sqrt{\sum_{t_k = t_i + \Delta t}\left(F^\gamma\left(t_k\right) - \langle F^\gamma \rangle\right)^2 \sum_i \left(F^x\left(t_i\right) - \langle F^x \rangle\right)^2}} \tag{B.3}$$

The finer the bin size is chosen, the fewer coincident time bins are found. The error increases because the fluctuation of smaller binned measurements are larger and because less time-coincident bins are found. The error calculation of the empirical correlation function is described in Appendix A.

Correlation of the data recorded by CT1 and ASM in 2001

Fig. B.11 shows the correlation for time shifts between ± 40 days. In Fig. B.13 the RXTE flux and the CT1 flux are plotted against each other for time coincident bins and Fig. B.12 shows both lightcurves for comparison. For better visibility, only coincident time bins are included in the plot. Tab. B.3 shows the ***correlation for different bin sizes***. It ***increases*** with bin size.

Correlation of the data recorded by the ASCA x-ray satellite in 1998 and several Cherenkov-telescopes

In the introduction chapter the measurement of the ***ASCA x-ray satellite*** and several Cherenkov telescopes (Wipple, HEGRA, CAT) between April 23, 1998 and May 1, 1998 were already presented (see Fig. B.14). The ASCA measurement is significantly more detailed and precise than that of ASM. Unfortunately, the TeV data is presently very sporadic and contains large error bars. However, the ***correlation*** between the x-ray flux and γ-flux was also analyzed.

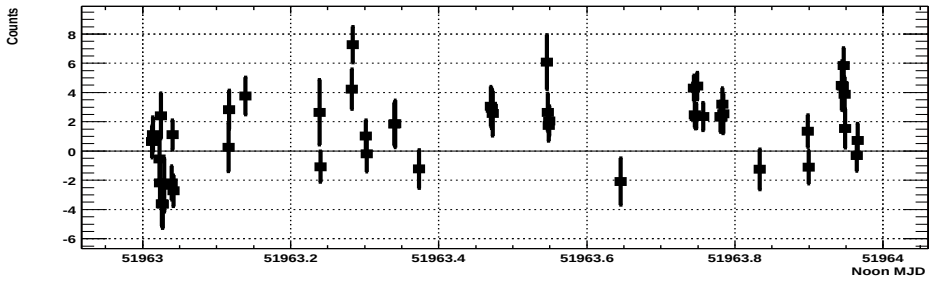

(a) ASM (one night)

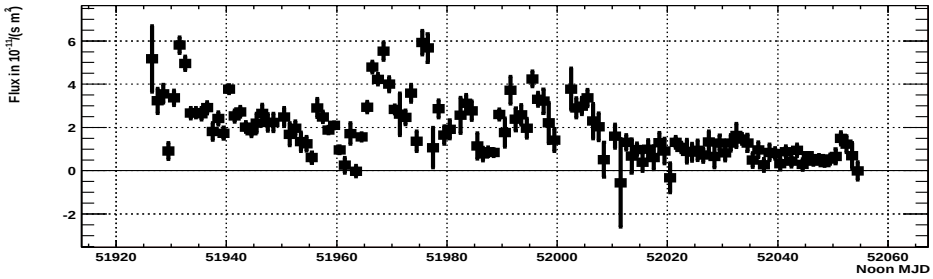

(b) ASM total period

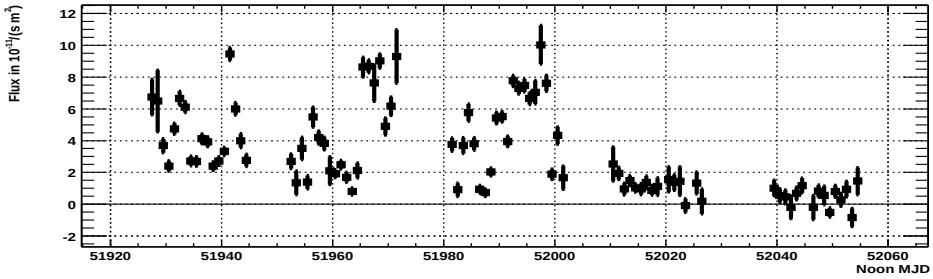

(c) CT1 total period

Figure B.10: The upper plot shows: a) A 24 hour sample of a ASM measurement for the day 51964. It can be seen that the ASM data is ***very noisy***. Almost simultaneous points show large differences. The middle plot shows: b)The light curve ***averaged over 12 hour bins***. The lower plot shows: c) The CT1 light curve for comparison. The ASM curve is continuous while the CT1 observation is interrupted by moon periods. From the upper two plots it is evident that while the ASM is very noisy when averaged over 12 hour bins it displays the ***trend*** of the flux. The flux outbursts seem to happen simultaneously for x-rays (ASM) and for γ-rays (CT1).

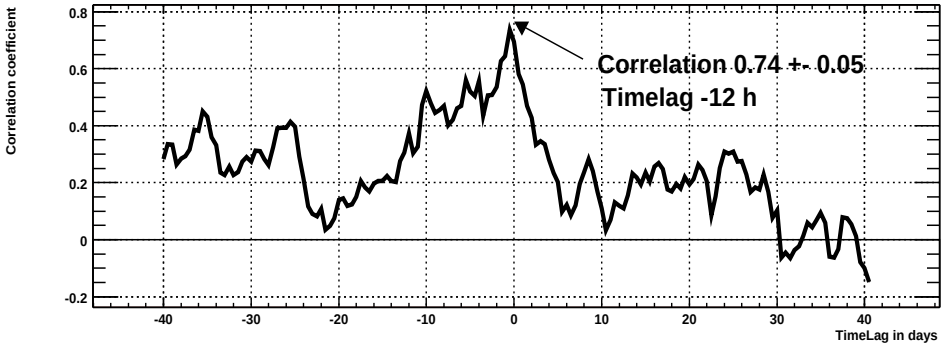

(a) ASM-CT1 correlation

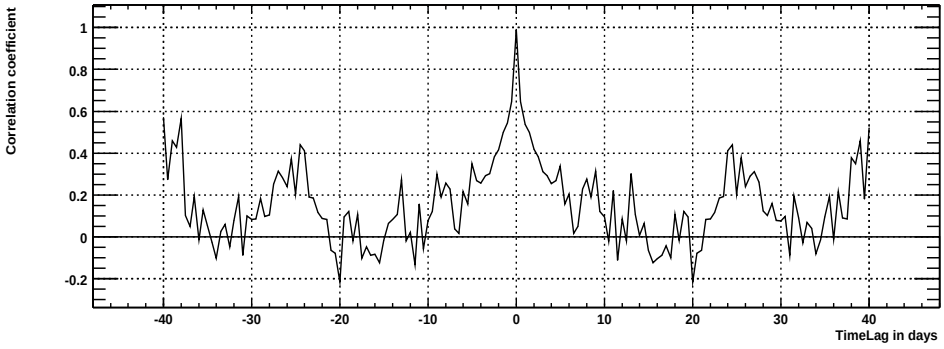

(b) Autocorrelation of CT1

Figure B.11: a) The upper plot shows the correlation between x-ray data and the γ-ray flux, as measured with CT1. The ***maximum correlation*** 0.74 ± 0.06 is reached at a time lag of the x-rays of -12h. It has to be mentioned that in this plot the timelag is not significant. The time lag will be discussed later in detail. The bin size was 1.0 days. To obtain a smooth curve, the time lag between bins was sampled in steps of 1/3 days. b) The lower plot is the autocorrelation of the CT1 data. The data seems to contain periodicities, which also appear in the upper plot.

Bin size (days)	Correlation
5.0	0.91 ± 0.07
2.0	0.83 ± 0.06
1.0	0.74 ± 0.05
0.5	0.73 ± 0.05
0.2	0.65 ± 0.05

Table B.3: The table shows the correlation for different bin sizes. It ***increases*** with bin size. It cannot be clarified in this thesis whether this has a physical origin or if this originates from larger errors when using smaller bin sizes.

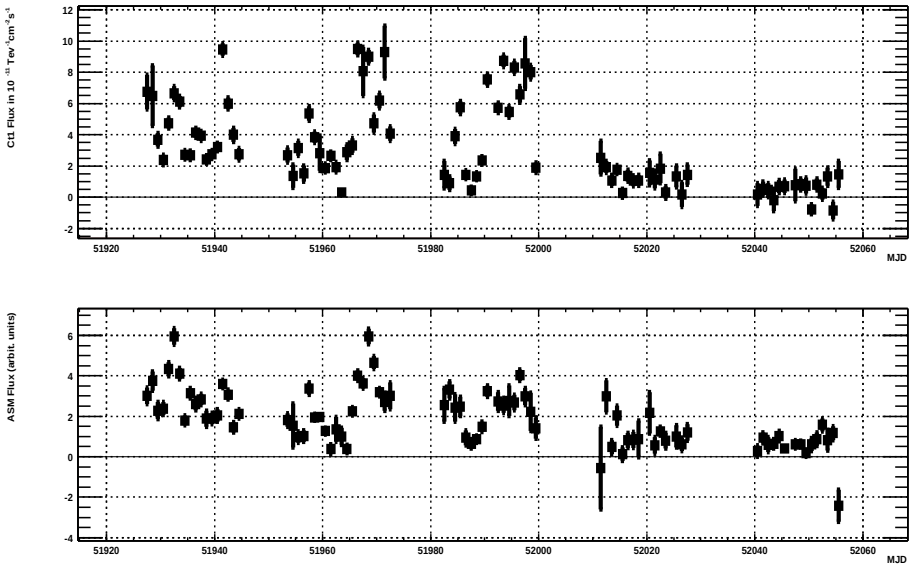

Figure B.12: a) The upper plot shows the CT1 flux and b) the lower plot shows the ASM flux. Note that, for better visibility only the time coincident bins of CT1 fluxes and ASM fluxes are plotted. The correlation is clearly visible now.

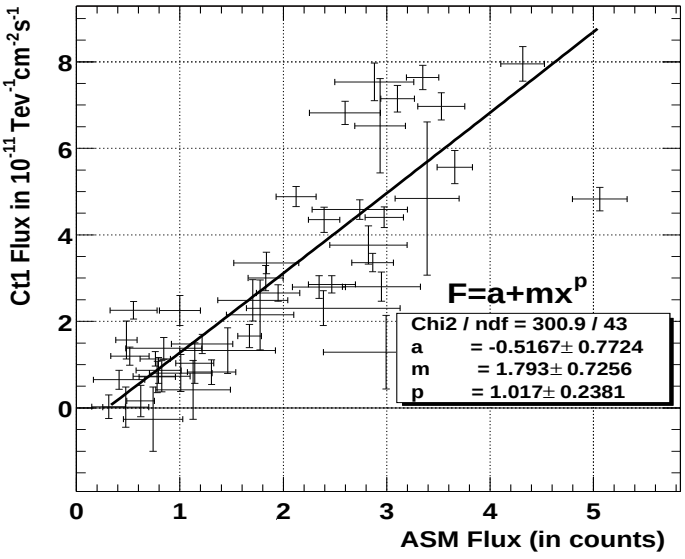

Figure B.13: In this plot the time coincident measurements are plotted against each other using a bin size of two days. The y-axis gives the CT1 flux in and x-axis the ASM x-ray flux in counts ($\propto$Flux). A function defined as $F = a + mx^b$ was fitted to the data. It reveals an ***almost linear*** dependence of the ASM flux on the CT1 flux , which is given by an exponent of b=1.0$\pm$0.2. The chisquare exhibits a large value since the correlation coefficient has a value of smaller than one (0.83 +- 0.06).

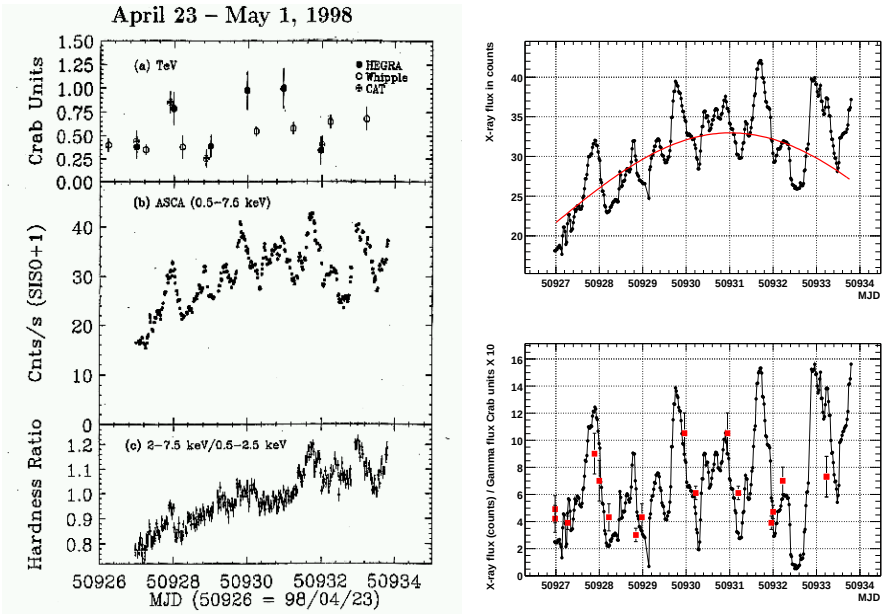

(a) Original ASCA measurement

(b) Subtracted background

Figure B.14: These plots show multiwavelenth measurements of Mkn 421 for the period between April 23, 1998 and May 1, 1998. a) The upper left hand plot shows TeV measurements by Wipple, HEGRA and CAT. The middle left hand plot shows x-ray measurements by ASCA. b) In the upper right hand plot the x-ray measurement is displayed with a background fit and the lower right hand plot shows the x-ray measurement with subtracted background and with superimposed TeV data points for illustration.